High temperature superconducting RF coil fabrication on flexible ceramic substrates for magnetic resonance imaging applications

(PN-III-P1-1.1-TE-2019-1777, Contract Nr. 191/2021)

Scientific Report

Contents

Project Objectives

”The objective of the project is the development of a thin film deposition technology for the growth of thin high temperature superconducting films on flexible ceramic substrates. The as-developed process will be used for the fabrication of radio frequency coils for magnetic resonance imaging applications.”

The objective of the project has been fulfilled, as we have developed thin film deposition processes for the growth of superconducting thin films on flexible ceramic substrates. These processes consist in:

- Planarization of flexible ceramic substrates;
- Deposition of a buffer layer architecture;
- Growth of superconducting $YBa_2Cu_3O_7$ thin films.

In the following, a detailed description of the above steps is presented. At the end of each section a brief description of the estimated results and achievements is given.

1. Solution deposition planarization of flexible, ceramic YSZ substrates

Coating solution synthesis and characterization

For the precursor solution preparation, yttrium acetate, $Y(CH_3COO)_3 \cdot 4H_2O$, was dispersed in methanol, CH_3OH, and dissolved in propionic acid, C_2H_5COOH. The concentration of the as-prepared solutions was 0.5 M and 1.5 M, respectively. The rheologic properties of the as obtained solutions were

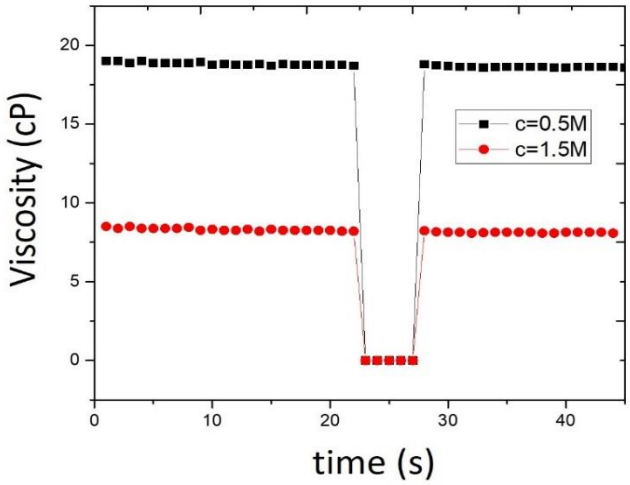

Figure 1. Evolution of precursor solutions viscosity with time.

investigated. The solution viscosity was determined using a DV1-Brookfield viscosimeter. The minimum solution volume for viscosity determination was 0.5 ml. The results obtained on the two solutions is presented in figure 1. As was expected the viscosity increases with solution concentration from 8.5 cP to 19 cP. Besides the concentration of the solution, viscosity is also influenced by the solvent content. It may be seen that there is little time variation of the viscosity around the mean value. This is an indication of the stability of the forces that sustain molecular agitation, which is desirable for keeping a high substrate wetting degree. The variation of the shear stress was investigated as a function of the shear rate for the c = 0.5 M solution. The linear dependence of the shear suggests a Newtonian fluid behavior of the precursor solution. The proportionality constant of the two physical quantities, which is the dynamic viscosity, η, was determined to be ~0.18 $(dyn/cm^2)\cdot s$.

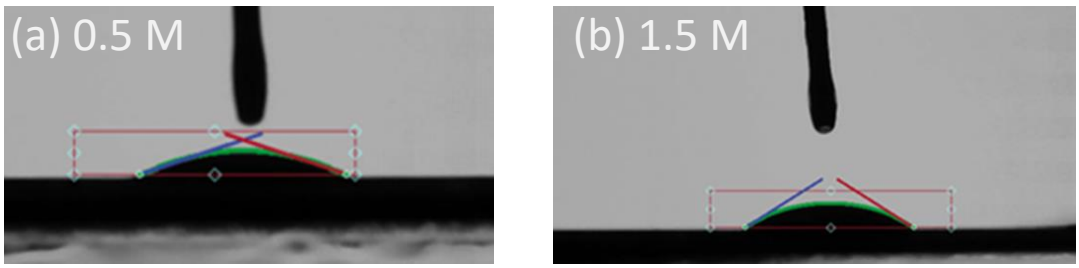

Figure 0-1. Wetting angle determination of the (a) 0.5 M and (b) 1.5 M precursor soultions.

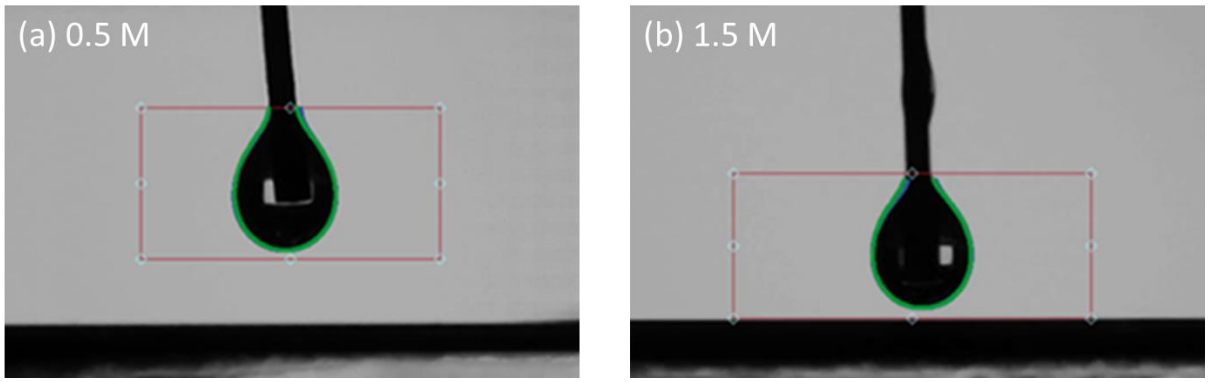

Figure 1.3 Surface tension determination for the (a) 0.5 M and (b) 1.5 M precursor solutions.

The wetting angle of the precursor solution was measured with an Ossila Contact Angle Goniometer, in a static regime. Within the same measurements, the surface tension of the solutions was also evaluated. The results are presented in figure 2. The obtained results are summarized in table 1. It may be seen that for the 0.5 M solution the wetting angle is quite low, 18.38°, indicating excellent wetting properties of the solution. Even the larger value, 32.2°, measured for the 1.5 M, suggests good prospects for a uniform substrate coating of the precursor solution.

Table 1. Contact angle and surface tensions of the precursor solutions.

Solution concentration (M)	*Contact angle (°)*	*Surface tension (mN/m)*
0.5	18.38	25.3
1.5	32.2	40.8

Optimization of the double-sided deposition process by dip-coating

Y_2O_3 thin film deposition on Al_2O_3 substrates

The present work package has the main objective the planarization of flexible ceramic substrates using a sequence of Y_2O_3 layer deposition. Due to issues concerning the commercial availability of flexible ceramic substrates, 0.15 mm thick, Al_2O_3 (Kerafol, Germany) substrates were used for preliminary planarization studies. The Y_2O_3 layers were grown by the chemical solution deposition method. The precursor solution was deposited on the alumina substrates by dip-coating. After the full substrate immersion in the coating solution, the samples were drawn at a constant rate of 1 mm/s. The as-obtained films were subjected to a thermal treatment, that was performed at 800 °C in oxygen atmosphere. The reason for this relatively high treatment temperature is to ensure that the subsequent thermal treatments of the following oxide layers, culmination with the $YBa_2Cu_3O_7$, which is treated in the range between 815 °C and 835 °C, do not affect the stability of the layers. Since the planarization layer structure constitute the thickest element of the final heterostructure, its thermal stability is paramount for the subsequent film growth. The morphology of the planarization films was investigated using a Veeco Dimension D3100 atomic force microscope. The investigated samples consisted of a Y_2O_3 thin films obtained using both the 0.5 M and the 1.5 M precursor solution. Two

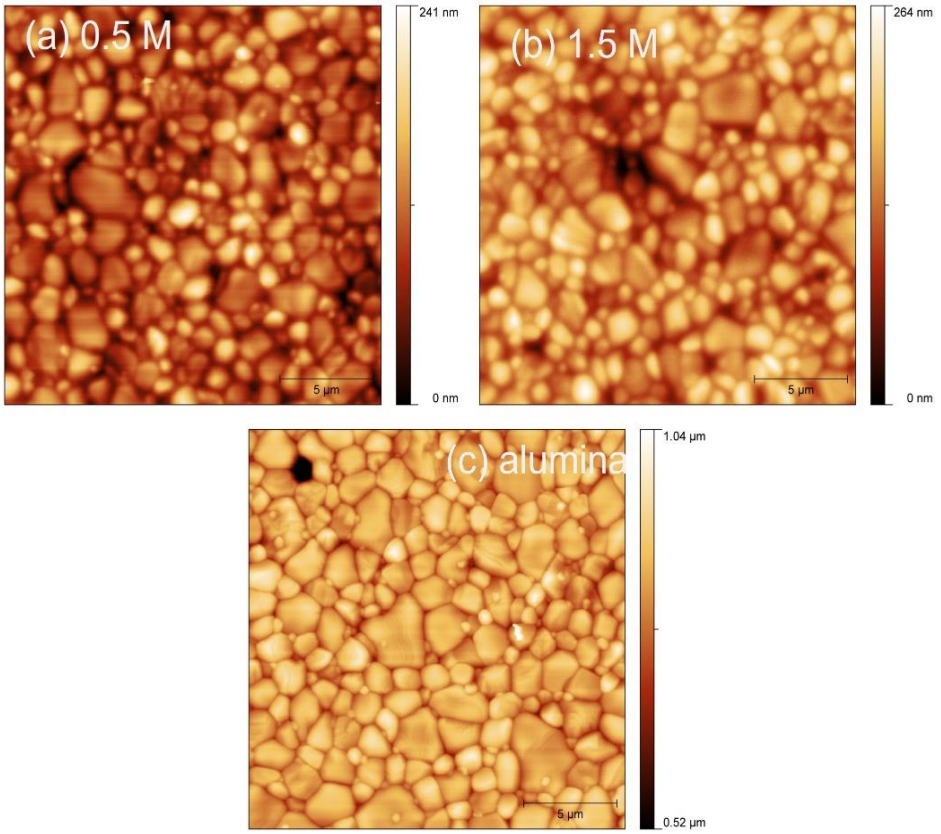

Figure 3. 20 µm × 20 µm AFM images of the yttria planarization bi-layers obtained from the (a) 0.5 M and (b) 1.5 M solution concentrations. (c) Alumina substrate reference.

layers for each sample were deposited by dip-coating (1 mm/s withdrawal rate). After the first deposition the as-obtained films were dried at 100 °C. After the second layer deposition, the bi-layers were annealed at 800 °C in oxygen atmosphere for 1 hour. The obtained results are presented in figure 3. The morphological parameters are summarized in table 2.

Table 2 Morphological properties of the planarization layers.

Sample	*RMS roughness (nm)*	*Maximum height (nm)*	*Average height (nm)*
Alumina substrate	58	1148	841
Y_2O_3 (c = 0.5 M)	34.3	253	111.9
Y_2O_3 (c = 1.5 M)	35.7	264.5	145.9

It may be observed that even with just two coatings the morphological properties of the planarization layers are dramatically improved with respect to the alumina reference substrate, with a decrease of about 40 % of the RMS roughness and a reduction of the average height by 7.5 times, in the case of the 0.5 M film. Similar values are obtained for the 1.5 M film. Thus, so far, it may be concluded that the yttria films indeed act as a planarization layer, even though several additional coatings are needed to further improve the surface quality. No significant difference is observed when using different concentrations of the precursor solution concentration.

Y_2O_3 thin film deposition on YSZ flexible substrates

The Y_2O_3 precursor solution described earlier was deposited by dip coating on flexible YSZ substrates (ENrG, USA closed) with a substrate immersion and withdrawal speed of 1 mm/s. The corresponding thermal treatment of the as-deposited films consisted of a slow heating ramp of 5 °C/min up to 400 °C. This first step was performed to promote precursor decomposition and organic part elimination.

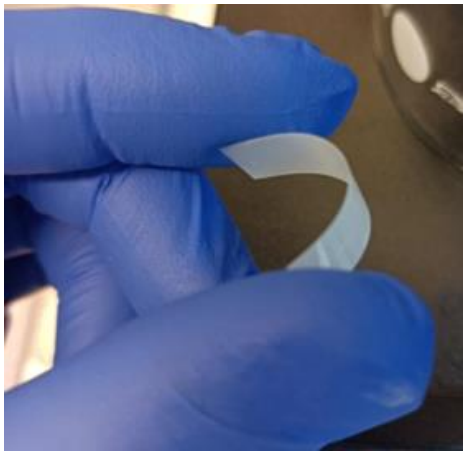

Figure 4. Image of the YSZ flexible substrate.

The crystallization of the films was obtained at 700 °C following a 10 °C/min heating ramp and a dwell time of 1 h. The structural characterization of the planarization layers was performed by X-ray diffraction measurements, figure 5. The additional X-ray peaks corresponding to Y_2O_3 confirm the fact that indeed the crystallization step was effective for obtaining Y_2O_3 thin films. In terms of film morphology, figure 6, a comparative study between the bare substrate and the Y_2O_3 layer revealed only a minor role of the film in the planarization of the substrate. The RMS value of the film roughness

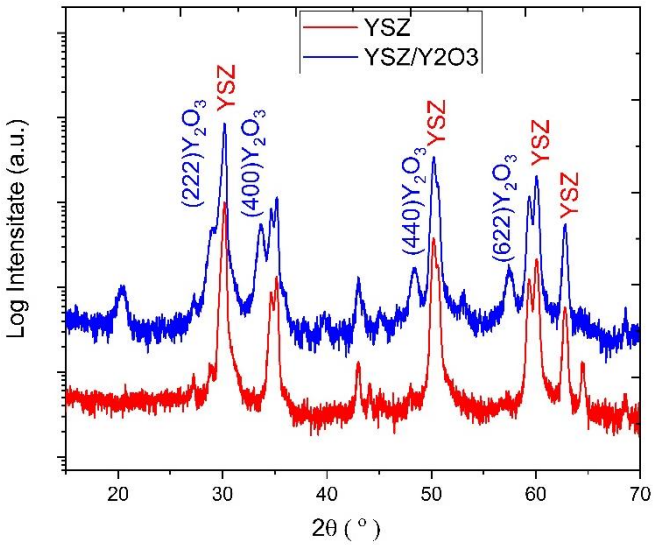

Figure 5. Typical X-ray diffraction of YSZ/Y2O3 film and YSZ substrate.

increases with respect to that of the substrate, from 27,2 nm to 31 nm. This may be due to the morphology of the film itself, however, it may also originate from the particular investigated area of

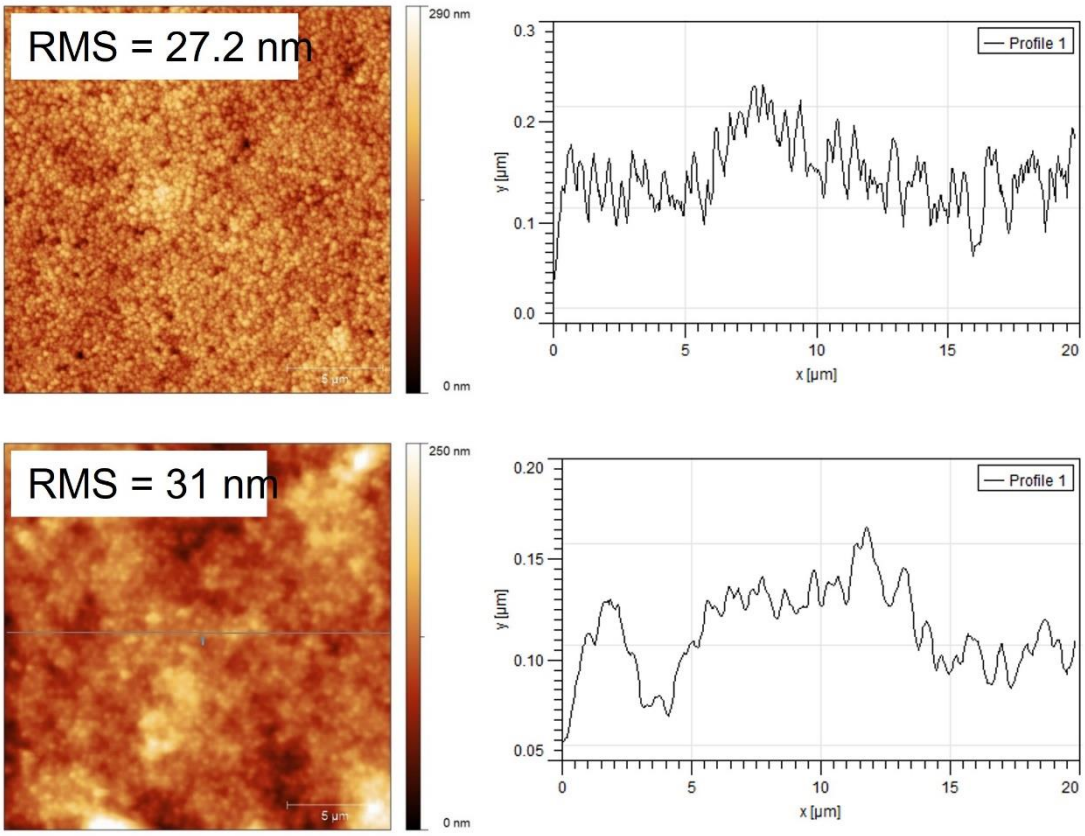

Figure 6. 20 µm × 20 µm AFM images of the YSZ substrate (top) and the Y2O3 film (bottom) and the corresponding profiles.

the sample. To support this, the surface profiles presented, show that upon the film deposition the short-range surface roughness tends to be eliminated, leaving just the long-range surface variation, *i.e.* waviness, which in principle is not detrimental to the subsequent buffer layer growth.

To improve the planarization properties of the Y_2O_3 layer, various quantities of glycerol (5, 10 and 20 % vol.) were added to the Y_2O_3 precursor solution. The latter had a concentration of 1.5 M. The as-obtained solutions were characterized in terms of viscosity, substrate contact angle, and surface tension. The results are summarized in the table below. An increase of all three investigated parameters is visible upon the increase of the glycerol content.

Table 3. Rheologic parameters of the coating solutions

Solution	*Viscosity (cP)*	*Contact angle (°)*	*Surface tension (mN/m)*
Y-Prop	19.2	32.2	25
Y-Prop 5% Glycerol	25.4	34.5	35.5
Y-Prop 10% Glycerol	28.5	35.6	40
Y-Prop 20% Glycerol	33.8	37.7	55

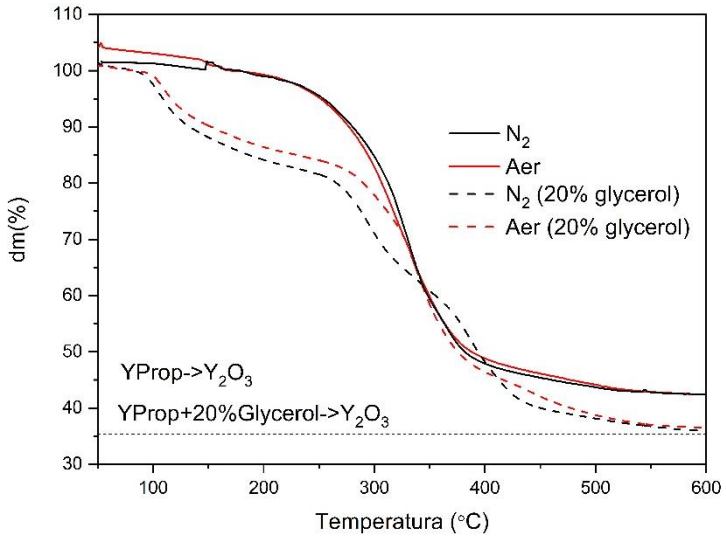

Figure 7. Thermo-gravimetric analysis of the Y-Prop and Y-Prop + 20 % vol. Glycerol coating solutions.

To correctly define the appropriate thermal treatment of films deposited by the chemical solution deposition techniques the precursor solution thermal decomposition must be investigated. In figure 7, the thermo-gravimetric (TG) curves are presented for the Y-prop and Y-prop + 20 % vol. glycerol precursor powders. The investigations were performed in an N_2 atmosphere and in air. In case of the Y-prop solution the decomposition takes place in a single step, between 250 – 400 °C. No significant variations were recorded between the decompositions in N_2 and air, respectively. The addition of glycerol in the precursor solution determines the presence of additional decomposition steps in the 100 – 150 °C and 300 – 450 °C intervals, attributed to the glycerol decomposition. An interesting feature is observed between the N_2 and air measurements. In N_2 an additional process is observed, starting at 350 °C, which has no direct correspondence in the case of the air treatment. Some indication of a decomposition process in air is visible at 400 °C, however the corresponding mass loss is significantly lower than that of the 350 °C step seen in N_2. Up to the present time, no explanation of these features exists and further studies are needed to elucidate these differences, *e.g.* thermo-gravimetric measurements coupled with mass spectroscopy, analysis of samples with different glycerol content. However, the conclusion of the above study is that for the growth of the Y_2O_3 films starting form a precursor solution with a 20 % vol. glycerol content, the thermal treatment consists of a slow 5 °C/min heating ramp up to 500 °C, for the decomposition and elimination of the organic part, and a crystallization step at 700 °C. The heating ramp up to the crystallization temperature is of 10 °C/min, while the dwell time is 1 hour. The thermal treatment is performed in N_2.

Following the treatment described above Y_2O_3 layers were deposited on the YSZ flexible substrates. To promote substrate planarization our study consisted of sequentially depositing Y_2O_3 layers, from 1 up to 4 layers. Each layer was subjected to the full thermal treatment. The results in terms of surface morphology are presented in the figure 8. It may be observed that the most significant drop in RMS

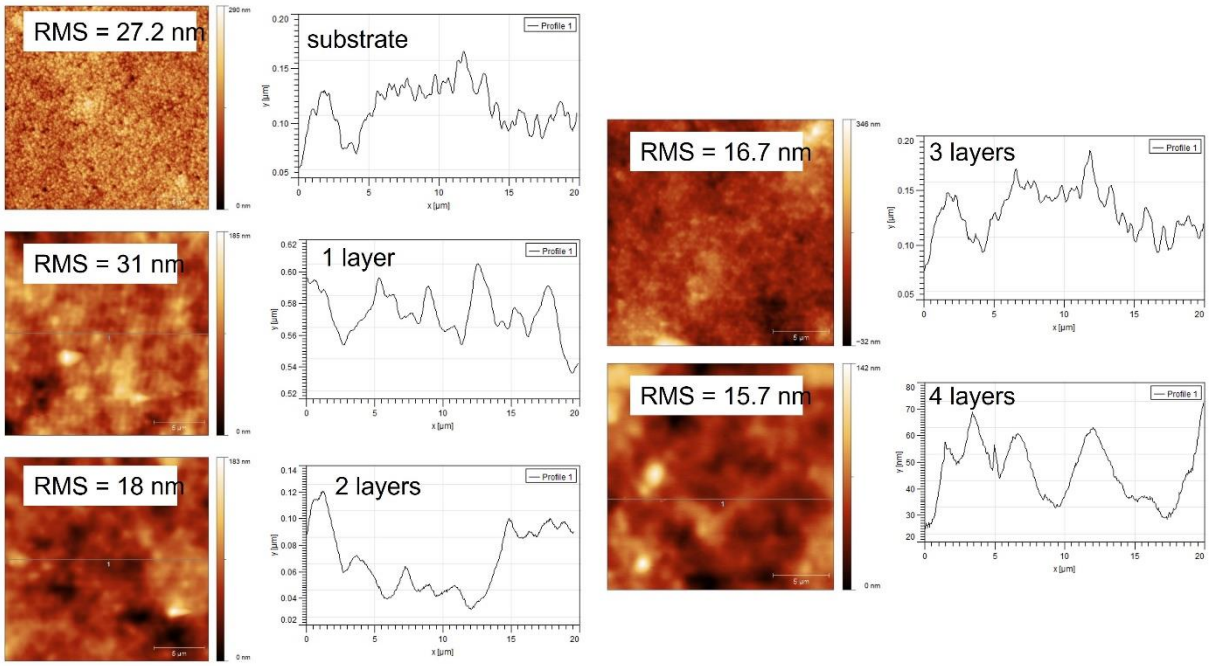

Figure 7. 20 µm × 20 µm AFM images of the YSZ substrate and the subsequent Y_2O_3 layers, with the corresponding profiles.

roughness is recorded after the deposition of the second step, from 31 to 18 nm. Afterwards, only a minor decrease is observed, reaching a value of 15.7 nm for the deposition of 4 layers. From the investigated AFM image profiles it is noticeable that the Y_2O_3 layer growth leads to an elimination of the short-range roughness. However, the long-range roughness is still present and the final value of 15.7 nm is still high, in literature values of 2-3 nm are reported.

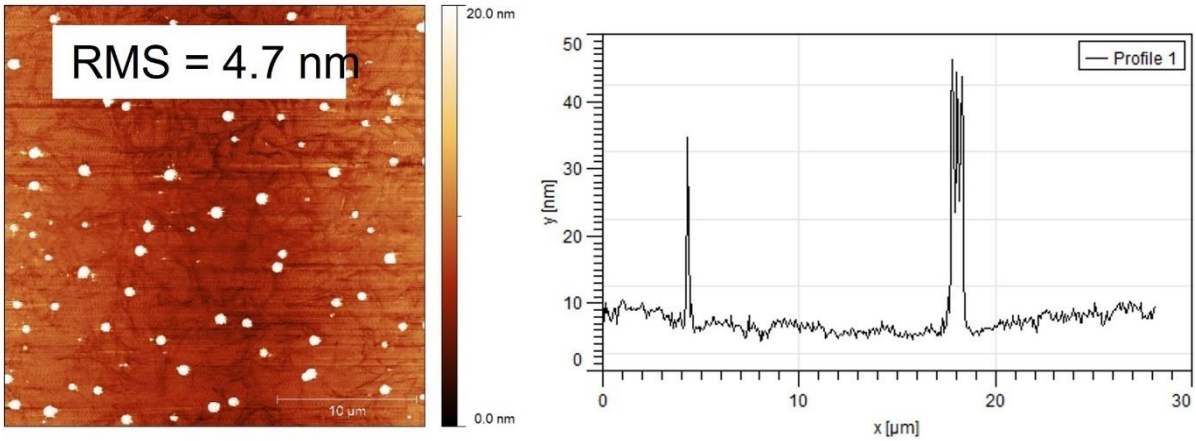

Figure 8. 25 µm × 25 µm AFM images of the Y_2O_3 obtained after the functionalization of the YSZ substrate.

In an effort to further decrease the RMS roughness of the Y2O3 layers an alternative deposition approach was proposed. It consisted in the functionalization of the YSZ substrate with tetraethoxysilan (TEOS). In the first step a TEOS/alcohol solution was prepared by mixing TEOS with ethanol in a ratio of 3:10 and subsequent ammonia addition, 50 ml. The solution was deposited on the YSZ substrates which were then treated at 200 °C for 1 hour. After the surface functionalization, Y-Prop 20% Glycerol

coating solution was deposited and the Y2O3 films were obtained following the previously reported thermal treatment. The AFM image, figure 8, show a decrease of the surface roughness down to 4.7 nm. Low-density, large particulates having a height 40-50 nm and a diameter of several hundred nanometers are seen on the films surface.

Estimated results and achievements This activity has been successfully completed as it was demonstrated a reduction of the RMS roughness value of the YSZ substrates from 27.2 nm to 4.7 nm.

2. Deposition of the buffer layer architecture, $YBa_2Cu_3O_7$ thin films and RF coil fabrication.

MgO buffer layer deposition

For the epitaxial growth of YBCO thin films a buffer layer stack is needed to ensure a suitable crystalline template as well as a good surface morphology. By means of the inclined substrate deposition method (ISD) the epitaxial growth of the MgO layers is promoted. This method consists in the e-beam evaporation of a MgO target material on a substrate that is oriented at an angle with respect to the

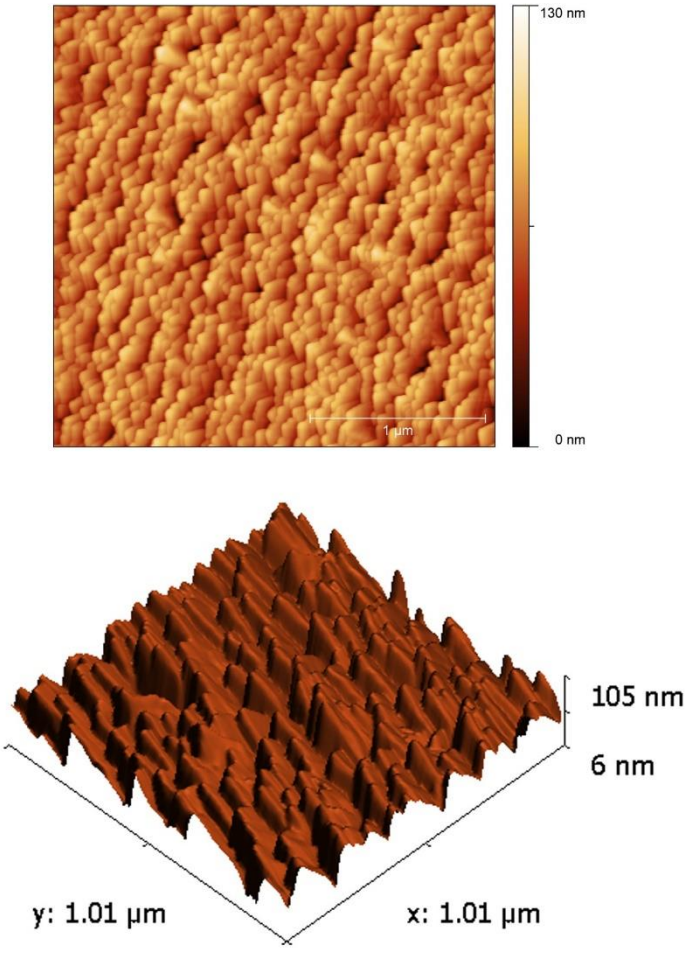

Figure 9. 2.5 µm × 2.5 µm of the MgO layer obtained by inclined substrate deposition method (top), 3-D image of the MgO film morphology (bottom)

incident evaporated material flux. In our case, we used a Si/SiO2 substrate, for which the amorphous

SiO2 layer was obtained by a suitable thermal treatment. The deposition parameters of the MgO layers consisted in a base pressure of the deposition chamber of 2 × 10-7 Torr, an angle between of 45° between the substrate and the MgO flux, and a deposition rate of 50 nm/s deposition rate. The high deposition rate determines the preferential growth of oriented MgO crystallites. The MgO film thickness was 1 µm. The AFM images, figure 9, exhibit a typical surface morphology for ISD-MgO films. It consists of rectangular crystallites that are oriented at an angle with respect to the substrate surface. The RMS roughness was of 13,9 nm and a peak-to-valley value of 113,3 nm.

$LaMnO_3$ buffer layer deposition

The final buffer layer prior to the YBCO growth consisted of a $LaMnO_3$ (LMO) film deposited using the chemical solution deposition method. For the preparation of the precursor solution lanthanum and manganese acetylacetonates were mixed in the appropriate stoichiometric ratio. The two solutions were obtained by mixing $La(CH_3COCHCOCH_3)_3 \cdot xH_2O$ and $Mn(CH_3COCHCOCH_3)_3 \cdot xH_2O$ in an excess of propionic acid. The concentration of the precursor solution was 0.8 M. After the spin-coating of the

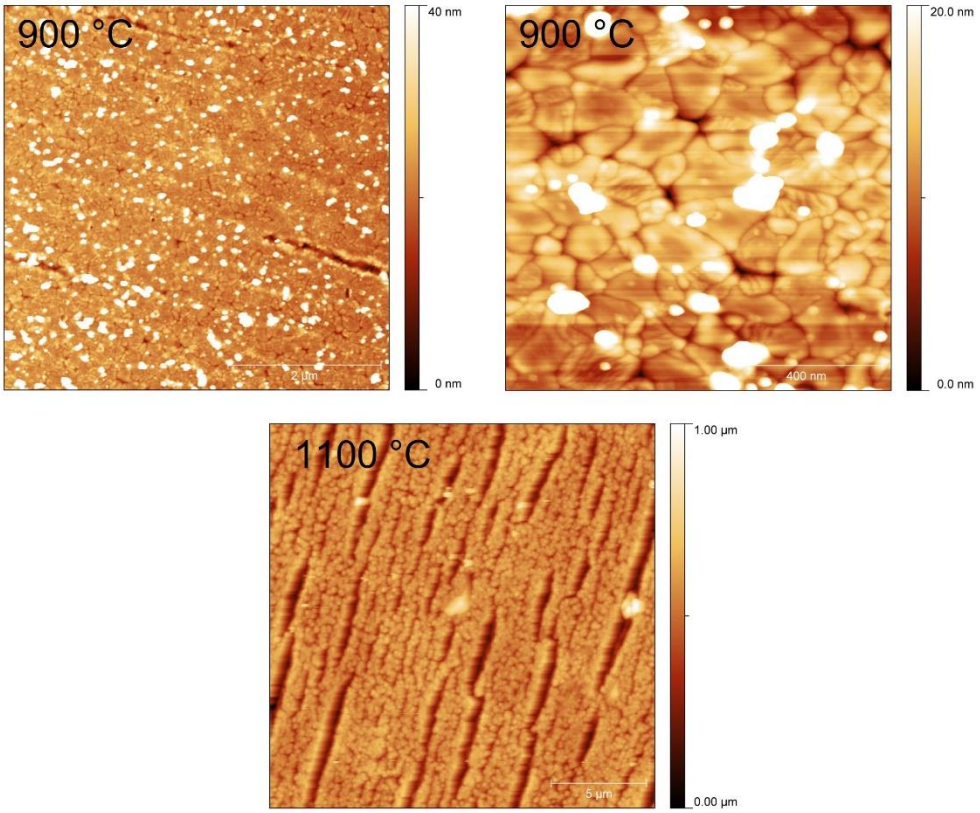

Figure 10. 5 µm × 5 µm and 1 µm × 1 µm images of the LMO thin film deposited on MgO buffer layer at 900 °C (top), 5 µm × 5 µm image of the LMO thin film deposited on MgO buffer layer at 1100 °C (bottom)

LMO solution on the MgO buffer layer, it was subjected to a thermal treatment. The treatment was performed in air and consisted of an initial heating at 600 °C with a low heating rate, 5 °C/min. This step ensures the decomposition of the precursor gel, without generating cracks or porosity in the final film. The crystallization step was performed at temperatures in the 800 – 1100 °C range. Although

several tests were performed by depositing the LMO films on MgO (001) single crystal substrates, here we present the results obtained on the films deposited on the MgO-ISD template. In the figure 10 the AFM images are presented for LMO deposited at 900 °C and 1100 °C, respectively. It may be seen that the best result obtained in terms of morphology is obtained for the layer grown at 900 °C. It exhibits an exceptionally low roughness of 2,3 nm, with a peak-to-valley value of 40 nm. In the situation of the film grown at 1100 °C the situation is opposite, in the sense that the film has a high roughness, 90 nm. Also, due to the high growth temperature, the film exhibits extend cracks throughout the film surface, with a height of approximately 1 μm.

$YBa_2Cu_3O_7$ layer deposition and characterization

Experimental

The YBCO fluorine free coating solution was prepared using cost effective metal acetate precursors $Y(CH_3COO)_3 \cdot 4H_2O$, $Ba(CH_3COO)_2$, $Cu(CH_3COO)_2$ (Alfa Aesar, Germany) in a stoichiometric ratio Y^{3+}: Ba^{2+}: Cu^{2+} = 1:2:3. Afterwards, the precursors were individually dissolved in methanol (Alfa Aesar, Germany) and propionic acid (Alfa Aesar, Germany). For the $Ba(Ac_2)$ and $Cu(Ac_2)$ mixture, NH_4OH 32% (Merck, Germany) was added dropwise until the solution became clear. All these procedures were performed in an ultrasonic bath. In the next step, the solutions were mixed together, stirred for 10 minutes and concentrated by evaporation. The water was evaporated at 75 °C and methanol at 58 °C by using a Büchi R215 rotary evaporator. After the evaporation process, the obtained blue marine coating solution was cooled down to room temperature until the next day. Subsequently, 10% vol. of diethanolamine (DEA, >99%, Fluka, Switzerland) was separately added to improve the solution viscosity and stability. The precursor solutions concentration was 1.1 M. Finally, the solution was deposited by the spin coating method (VTC-100 Vacuum Spin Coater) on 7.5mm × 7.5mm $SrTiO_3$ (STO) substrate at a 3000 rpm for 60 s. An important step for a quality coating and surface wettability is the cleaning process of the substrate surface. Cleaning has been performed by sonicating the substrate for 3 minutes in an aqueous solution of nitric acid, followed by 1 minute in isopropanol. After coating, the amorphous film has been subjected to an optimized double-step thermal treatment process. The films were pyrolyzed in a tubular furnace, the temperature was increased from room temperature up to 600 °C with a dwell time of 60 minutes, in humid O_2 flow (20 l/hour). Subsequently, the YBCO growth took place at 835 °C at a heating rate of 20 °C/min, for 180 min in a humid N_2/O_2 atmosphere. The orthorhombic symmetry is developed during the oxygenation at 450 °C on the cooling ramp by maintaining the sample at this temperature for one hour in an oxygen flow.

The thermal decomposition of the precursor powder was performed using thermogravimetric-differential thermal analysis (TG-DTA) coupled with quadrupole mass spectrometry (QMS 200) atmospheric sampling system (Residual Gas Analyzer RGA-Stanford Research System) to reveal the gas

species involved during decomposition with m/z=10-90 a.m.u. The analysis was carried out in a humid O2 atmosphere up to 800 °C. The powders were obtained by drying the coating solutions on a hot plate between 50-70 °C. The temperature is adapted to the nature of the added chelating agent. Next, the powder was kept for one hour under vacuum in a dry oven at 70 °C, afterwards grinded in a mortar and pestle. Alumina was used as the reference material.

Infrared analyses of precursor solutions were performed by Fourier Transform Infrared Spectroscopy (FTIR, Bruker Tensor 27) in the range between 500 and 2000 cm^{-1} with a resolution of 4 cm^{-1} with 32 scans for each sample.

The structural characterization of the YBCO thin films was performed by X-ray diffraction, 2θ/ω and ω-scans, using a Bruker D8 Discover diffractometer (Cu Kα radiation). The electrical characterization of the superconducting properties (R(T,B), Jc(T,B)) was performed in a Cryogenic Ltd. cryogen-free cryostat in the 4.5-77 K and 0-18 T temperature and magnetic field interval, respectively. For I-V transport measurements films were patterned using standard UV photolithography and wet etching to obtain 1 mm long strips with a width of 30 and 50 µm. The critical current density was estimated from the V(I) characteristics using a 1 µV/cm criterion. Magnetization measurements were performed by SQUID (Quantum Design, San Diego, CA) and the Bean critical state model was used to extract the critical current density of the film.

The morphological properties of the film were analyzed by optical microscopy (Zeiss), and atomic force microscopy (AFM-Vecco). The microstructure of the thin film was identified by transmission electron microscopy (TEM), using a JEOL JEM-2100F microscope operated at 200 kV. For TEM sample preparation we used a HELIOS NanoLab 600 instrument, with cutting, thinning, and polishing with a gallium liquid metal ion source at 30 kV acceleration voltage and different probe currents (21 nA, 6.5 nA, and 28 pA). Finally, the resulting TEM lamella dimension is approximately: length = 8 – 10 µm, width = 5 – 6 µm, and thickness = 60 – 100 nm.

Infrared spectroscopy characterization of the precursor solution

To reveal a possible reaction of the organic additive with the YBCO precursor solution, we have performed the FT-IR measurements presented in Fig. 2.1. The stretching vibrations at 1541, 1412, and 1284 cm^{-1} are characteristic to the asymmetric $\nu_{(as)}$, symmetric $\nu_{(s)}$ carboxylic groups $\nu(COO^-)$ to νCH_2, respectively. Moreover, the coordination mode of the propionate groups can be deduced from the difference of the asymmetric and symmetric absorption of $\nu(COO^-)$ [$\Delta\nu = \nu_{as}(COO^-) - \nu_s(COO^-)$]. In our case, the difference $\Delta\nu = 129$ cm^{-1} indicates a bidentate chelating ligand which binds one or two cations. The presence of this structure makes the solution more robust, by hindering the coordination of water molecules. The peak groups appearing at 1461 and 1020 cm^{-1} are the characteristic vibration modes of the methyl groups, attributed to CH_3 and CH_3O radicals. The characteristic band of free carboxylic acid $\nu(C=O)$ occurs at 1709 cm^{-1}, and νCH_2-CO-O appears at 1220 cm^{-1}. The absorption peaks below 650 cm^{-}

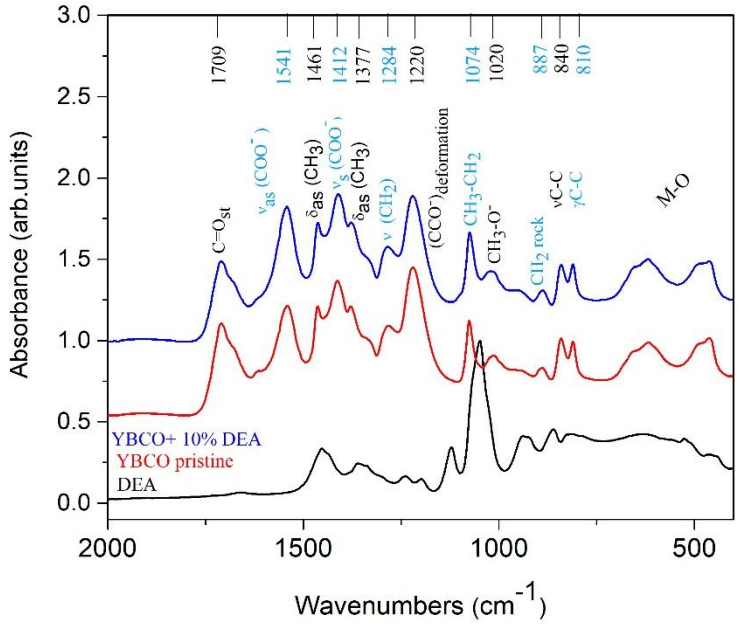

Figure 2.0-1 FT-IR spectra of the precursor solutions YBCO pristine (red), YBCO+10%DEA (blue) and DEA (black).

[1] are associated with M-O stretching vibrations. Additionally, the band of ammonia is absent from the spectrum of the precursor solution due to the evaporation process (see experimental methods). The peaks were assigned based on previous literature studies. The spectra of the YBCO solution with DEA nearly coincides with the YBCO pristine solution. No modification of the relative intensity of the YBCO-DEA peaks in the 900-400 cm^{-1} range, demonstrates that no complexation of DEA occurs with the metal ions.

Thermal decomposition of precursor powders

The decomposition behavior was studied by thermal analysis to optimize the thermal treatment profile for the thin film growth. In Fig. 2.2(a) we have plotted the mass variation of the precursor powders (i) with DEA (YBCO-DEA) and (ii) without DEA (YBCO pristine) heated at a 10 °C/min heating rate in humid oxygen atmosphere. It can be seen that the samples exhibit an almost similar pattern of the TG profile. The mass loss evolution has revealed that the decomposition occurs in three successive stages. This is also confirmed by the three peaks present in the DTA spectra, Fig. 2.2(b), which occur at different temperatures for the two samples. In the first stage, between 47-187°C the process displays a single endothermic peak for both samples at 41°C (YBCO pristine) and 47°C (YBCO-DEA), respectively, associated with the adsorbed water evaporation, according to the QMS measurements presented in Fig. 2.2(b) for the sample with DEA. From the initial weight, this corresponds to a 4% weight loss.

The second stage, registered in the 187-350 °C temperature range, is equivalent to a mass loss of 31 % for the pristine powder, and 36 % for YBCO-DEA, respectively. The DTA curve shows an exothermic effect at 270°C (YBCO-DEA), and 282°C (YBCO pristine). In the case of YBCO-DEA, this step

is attributed to the boiling point of DEA, and also related to the complete chelating process (with loss of gaseous NOx).

The complete decomposition reaction occurs by forming CO_2, NO_2 and H_2O volatile products. However, the high boiling point may promote a higher polymerization degree. Different degree of

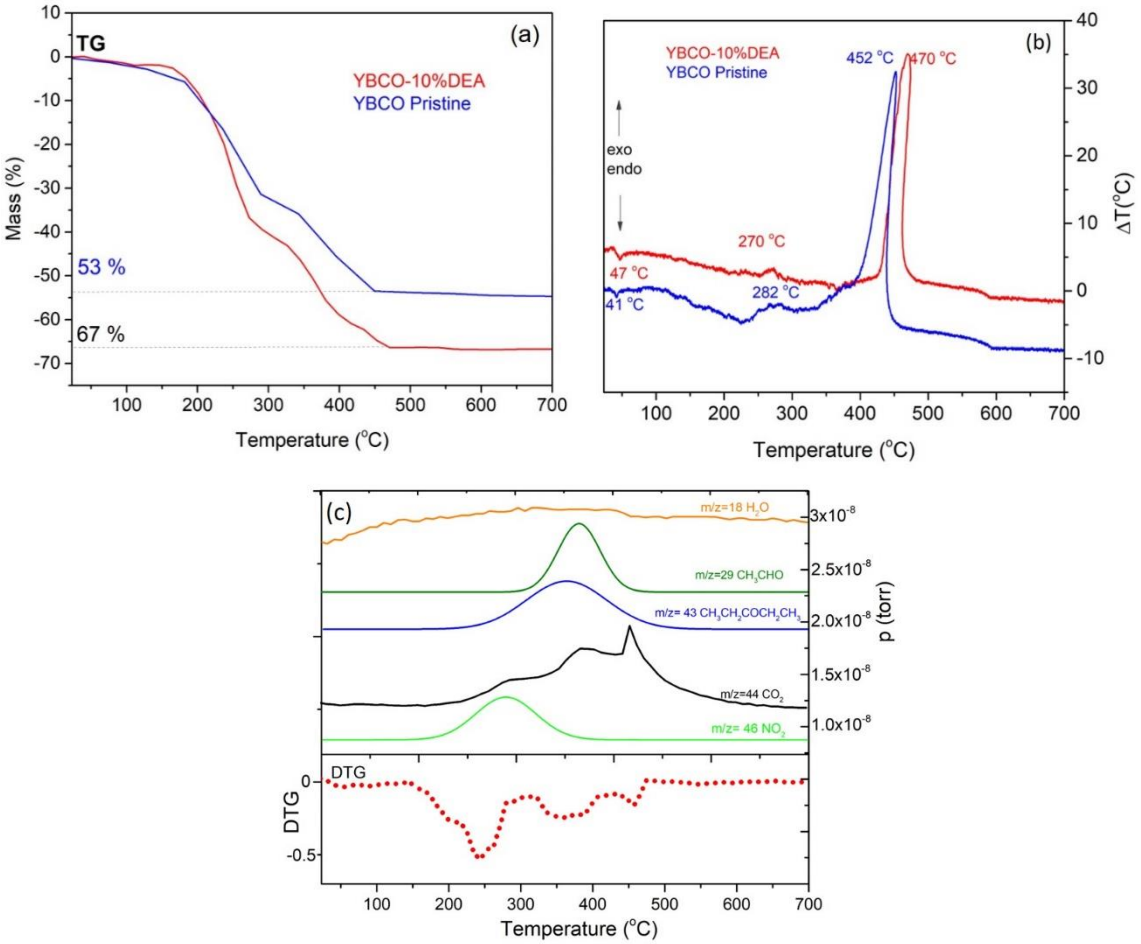

Figure 2.0-2 (a) TG and (b) DTA during decomposition at 10°C/min in humid O_2 atmosphere, and (c) the corresponding MS spectra of solid powder with DEA (YBCO-DEA).

polymerization due to the molecules of the chelating agents can affect the pyrolysis process of the thin films, which is the transformation of gels in an amorphous state. This can be explained in terms of nucleation and growth process.

The third stage (390- 600°C) is related to the precursors' decomposition evidenced by the exothermic peaks between 452-470°C. The fact that the peaks of the DEA- chelated precursor shift to higher temperature may demonstrate that the DEA solution has a chemical bonding to propionate groups. The total weight loss was 53% for pristine and 67% for YBCO-DEA, respectively. According to the TG curves the difference of the weight loss can be associated with the decomposition of metallic propionate. In the case of YBCO-DEA the MS (Fig. 2.2b) has revealed that the evolved gases correspond to the fragments with m/z= 43 characteristic for 3-pentanone ($CH_3CH_2COCH_2CH_3$), m/z= 29 for CH_3CHO

and m/z= 44 for CO_2. All these fragments correspond to the propionate decomposition [28]. After the precursor decomposition, above 600 °C the weight loss of the powder remains stable.

Precise elucidation of the decomposition process is hindered by the presence of three metal ions participating in the chelating process, with different ionic radii, *r*. These are 1.61Å, 0.87 Å and 0.99 Å for Ba^{2+}, Cu^{2+}, and Y^{3+}, respectively. The reactivity of metal cations in the formation of metal-chelate complexes may be influenced by the large differences in the ionic. Generally, the possible reaction between amine and carboxylate complex can be expressed as follows:

$$(Rx)_2NH + HOOC(R_Y) \rightarrow (R_x)_2NH_2{}^{+}{}^{-}OOC(R_Y)$$

where R_X is the alkyl substituent into the amine compound (ethyl or butyl). R_Y is the alkyl substituent into the acid compound (propyl, hexyl, or heptyl). In this work, diethanolamine (DEA) was used as the source of the cations, while carboxylate acids with alkyl chain length of propyl, was utilized to provide the anions of the complex.

Structural and morphological characterization

The physical properties of the as-obtained YBCO – 10 vol. % DEA thin films were investigated to assess the efficiency of the proposed approach in producing high performance superconducting YBCO thin films. The *2ϑ/ω* diffraction pattern of the film is presented in Fig. 2.3(a). It may be observed that the expected (001) texture of the YBCO film is present. Common issues affecting YBCO film epitaxy are the growth of crystallites oriented with the *a*/*b* axes perpendicular to the substrates, or poor overall film texture. These determine the presence of (*h*00) and (103) peaks, respectively in the X-ray pattern. No such features were observed in our measurement, as no additional peaks, besides the (00*l*) family, were recorded from the YBCO film. The out-of-plane *c* lattice parameter was evaluated using the Nelson-Riley method, to be 11.67 Å typical for YBCO thin films grown on STO (001) substrate. The lower value of the out-of-plane constant than its powder counterpart, 11.6802 Å, may be ascribed to the in-

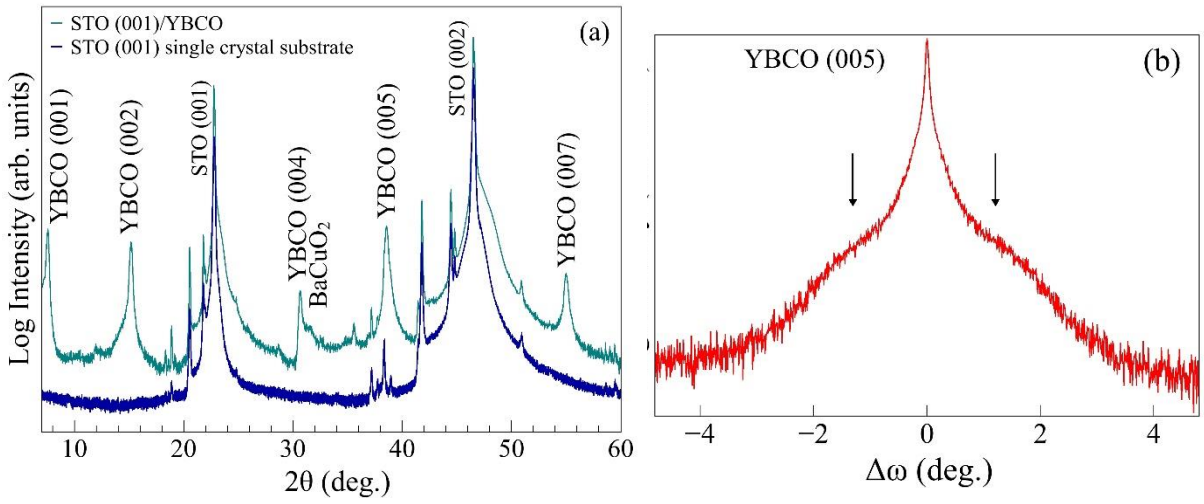

Figure 2.0-3 (a) 2ϑ/ω pattern for the YBCO thin film and the STO (001) single crystal substrate; (b) ω-scan around the YBCO (005) reflection (arrows mark the diffuse scattering peaks).

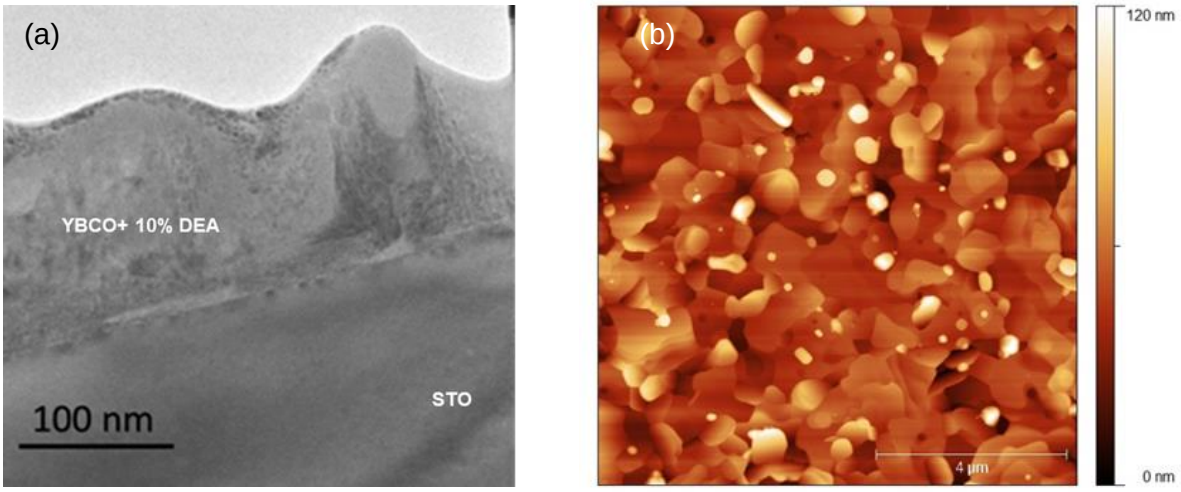

Figure 2.0-4 (a) TEM image and (b) 10 × 10 µm AFM image of YBCO-10 vol%.DEA film.

plane tensile strain present in the film. The cubic STO lattice constant is 3.905 Å, larger than both *a* and *b* parameters of YBCO leading to a mismatch of 1.56 %. Additional $BaCuO_2$ secondary phase was identified. For comparison, the X-ray diffraction pattern of the bare STO (001) single crystal substrate was added. The out-of-plane crystallite mosaicity was evaluated by performing an ω-scan around the YBCO (005) reflection, figure 2.3(b). The full-width at half-maximum (FWHM) of the as-obtained curve is 0.09°. The low value of the FWHM indicates a very narrow out-of-plane crystallite orientation distribution function. However, it may be observed that there is an additional, low intensity contribution, to the rocking curve, present in the form of symmetric shoulders, indicated by the arrows. In oxide epitaxial systems, such features are common. They may be explained on one hand by the existence of coherent diffraction on highly textured crystallites, responsible for the narrow high intensity peak. On the other hand, there is a diffuse X-ray scattering on local strain fields present around structural defects, which accounts for the low intensity component. The thickness of the as-obtained film was determined by means of transmission electron microscopy (TEM). The TEM image, Fig. 2.4(a), suggests a rather high thickness variation, with a minimum thickness of approximately 90 nm. The film is dense and shows a crack-free surface.

The surface morphology was investigated by contact AFM measurements on a 10 × 10 μm^2 area, Fig. 2.4(b). The surface morphology exhibits large flat crystallites with pores which may extend to the substrate surface. The presence of the large regular crystallites indicates a good crystallinity of the YBCO film, which, corroborated with XRD data demonstrated a good quality of the as-grown epitaxial YBCO film. Additionally, smaller round shape particulates grains are also visible. These are most likely amorphous phases such as: CuO, Y_2O_3, etc. Quantitatively, the root-mean-square (RMS) roughness was estimated to be 14 nm, while the peak-to-valley distance was >120 nm.

Superconducting transport properties

The temperature and magnetic field dependence of the resistivity, $\rho(T,H)$, of the YBCO film was studied near the critical transition temperature, T_c. The results are presented in Fig. 2.5. In zero magnetic field, the zero-resistance critical temperature, $T_c(R=0)$ is 88.1 K. The observed temperature-magnetic field dependence of the electrical resistivity is interpreted with the model of the thermally activated flux flow (TAFF), which well describes the broadening of the resistive transition and the decrease of T_c with the increase of the applied magnetic field. In the TAFF regime, for small current densities, $J << J_c$, the resistivity decreases exponentially as a function of temperature, according to

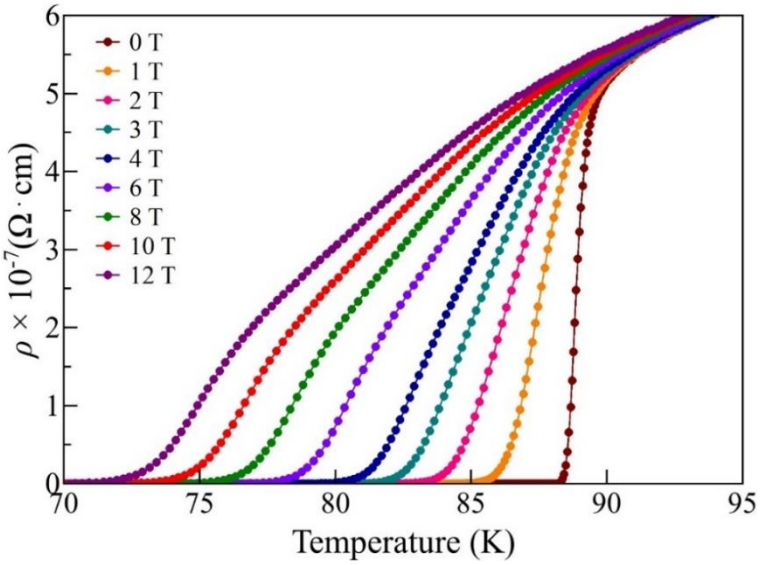

Figure 2.0-5 ρ(T) of YBCO thin film for various values of magnetic field showing the broadening of the resistive transition by magnetic field.

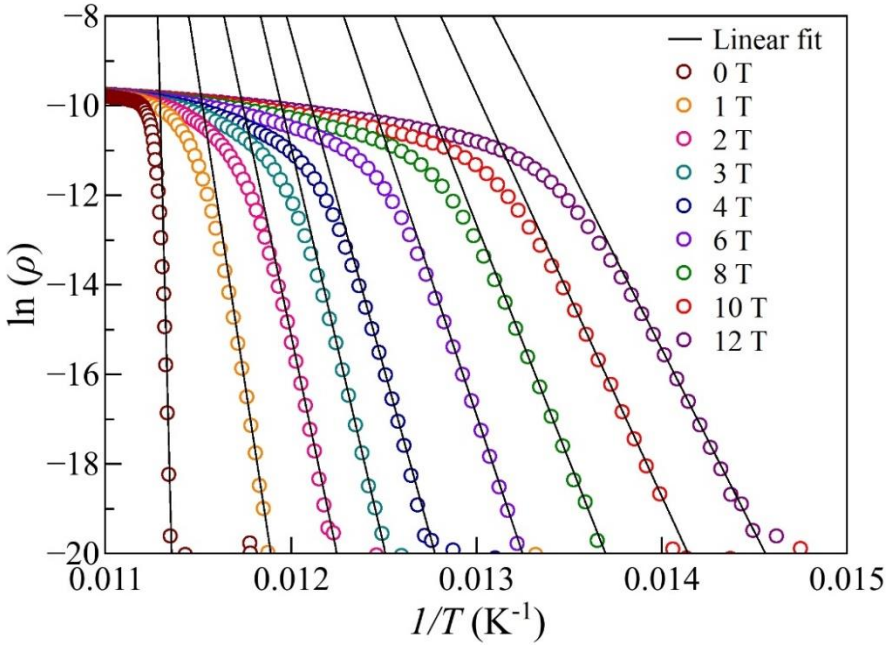

Figure 2.6 Linear fit of the ln(ρ) vs. 1/T dependencies.

$\rho(T,H) = (2\rho_c\, U/T)\exp(-U/T) = \rho_{0f}\exp(-U/T)$. *U* is the thermal activation energy (TAE), while the $2\rho_c\, U/T$ pre-factor is usually considered to be a constant, noted as ρ_{0f}. Usually, to calculate U_0, the *ρ(T)* data is plotted in an Arrhenius form ln(*ρ*) vs. *1/T*. The TAFF regime is situated in the linear part of the as obtained dependence. U_0 is determined as the slope of the linear regression of the experimental data, while the *y*-axis intercept is ln(ρ_0). As it may be seen from Fig. 2.6, a linear dependence of ln(*ρ*) as a function of *1/T* is observed in the TAFF regime. From the absolute values of the linear regression (solid lines), the slope U_0 was determined. In Fig. 2.7. the magnetic field dependence of the thermal activation energy is presented. The lack of additional pinning sites determines a rather steep decrease of the activation energy as a function of the applied magnetic field, especially at low fields.

One of the most important parameters in determining the superconducting transport performance is the critical current density, J_c. Its absolute value, together with its magnetic field and temperature dependence give a comprehensive image of the current carrying capabilities of a certain superconducting architecture. In Fig. 2.8, the magnetic field dependence of the J_c is presented at several temperatures. For comparison, the $J_c(\mu_0 H)$ at 77 K determined both by *V(I)* and magnetic SQUID measurements is shown. Transport measurements reveal a critical current density value in self-field of 3 MA/cm^2, while a slighter higher value, ~4 MA/cm^2, is registered from magnetization determination. The field dependencies of the two curves are relatively similar, both showing a steep decrease of the critical current density with the increase of the applied magnetic field. Since the magnetization measurements were performed on the entire sample, while the *V(I)* measurements were performed on patterned stripe, the similarity of the two magnetic field dependencies is an indication of the good

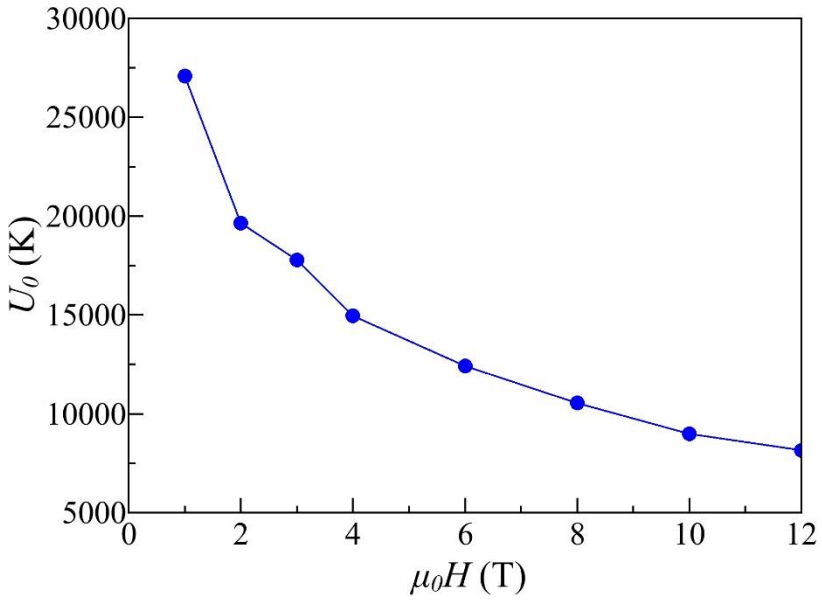

Figure 2.7 Thermal activation energy, U_0, as a function of the applied magnetic field.

homogeneity of the as-obtained film. The maximum pinning force density, F_p^{max}, was 0.95 GN/m^3, determined from transport measurements and 0.64 GN/m^3 from magnetization measurements ($F_p = J_c \times \mu_0 H$). No satisfactory fit was obtained for the data at 77 K using the power law decay, $J_c \propto H^{-\alpha}$. This may be ascribed to a low irreversibility field value, H_{irr} = 2.2 T (determined as the field at which the

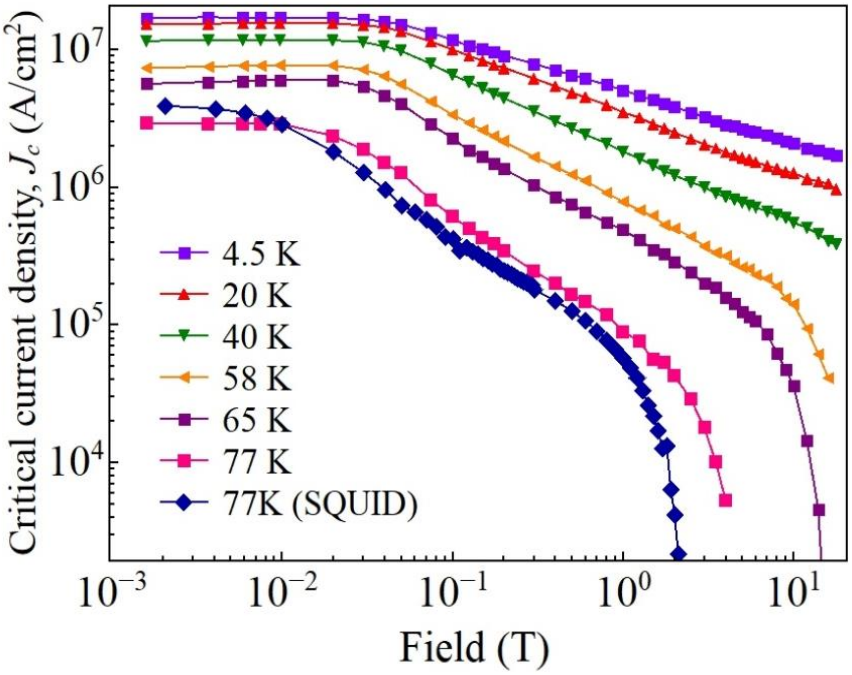

Figure 2.8 Magnetic field dependence of the critical current density at different temperatures

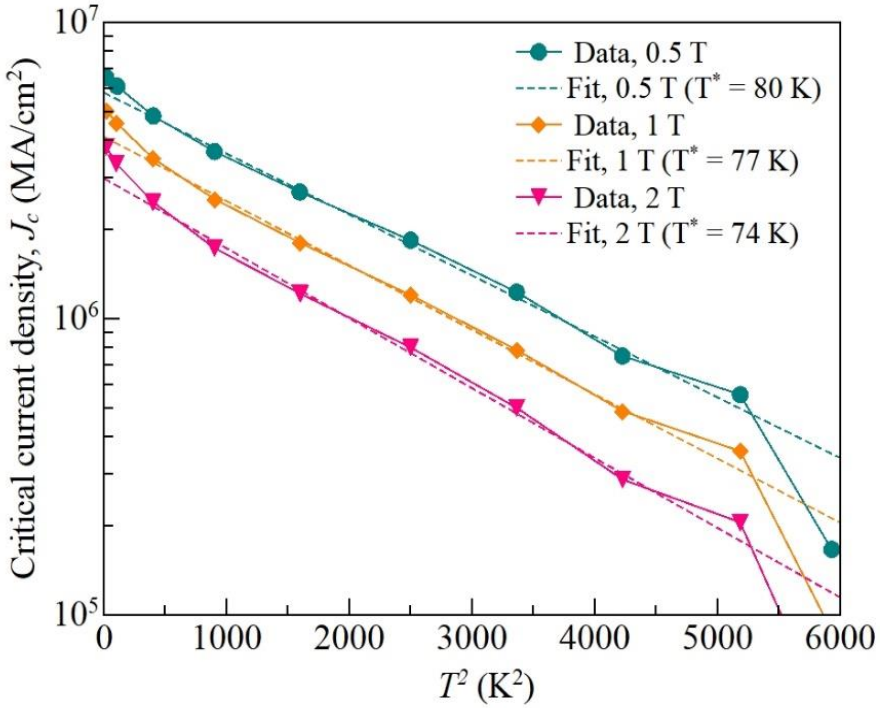

Figure 2.9 $J_c(T^2)$ dependencies at different applied magnetic fields, with the appropriate fits for the characteristic vortex pinning energy, T^* determination.

normalized pinning force decrease below 0.01), which in turn can be a result of the relatively low critical temperature. As expected, with the decrease of the temperature, thermal activation of the vortices is reduced, determining an increase of the critical current density in all the studied field range. At 4.5 K, for fields higher than 0.1 T, the power law describes well the $J_c(\mu_0 H)$ curve, with an exponent $\alpha = 0.35$. The low α value indicates that at low temperatures the film exhibits good vortex pinning properties. The above results suggest that the intrinsic occurring pinning centres within the film fail to provide sufficient pinning strength at high temperatures, *i.e.,* 77 K, but at the same time prove to be more effective in the low temperature range. Among the intrinsic pinning centres, the most important are point defects and twin boundaries. Due to the short coherence length in the HTSC the defect at a single atom site is sufficient to depress locally the superconducting parameters and, as a result, to act as efficient pinning centres. In an epitaxial YBCO film, the most common point defect is represented by the oxygen deficiency in the CuO_2 planes. It is to be noted that the density of this defect is strongly dependent by the film growth conditions.

The evolution of the critical current density as a function of the sample temperature was investigated at different magnetic fields ($H \,||\, c$) to assess the nature of vortex pinning present within the film. It has been shown that three types of pinning contributions may exist in epitaxial YBCO thin films classified according to their strength and direction of action. These are isotropic weak, isotropic strong, and anisotropic strong centres. The weak and strong contributions have specific temperature dependencies. In case of the strong populations the analytical expression for the critical current density is $J_c(T) \sim J_c(0) exp(3(T/T^*)^2)$, where $J_c(0)$ is the critical current density at 0 K, while T^* is a characteristic vortex pinning energy. In Fig. 2.9 the J_c is presented as a function of T^2, in logarithmic scale, at different applied magnetic fields. The data was fitted with the above expression, and it may be observed that for all investigated fields it closely follows the respective fits in the 20 – 65 K interval. This means that in the specified temperature regime the dominant contribution comes from a strong pinning population. The as-obtained T^* values started at ~80 K at 0.5 T and decreased to ~74 K at 2 T.. This contribution becomes dominant at high magnetic fields. The satellite peaks in the rocking curve pattern, confirm the existence of such correlated lattice defects and therefore explain the observed strong pinning contribution. However, it is to be noted that ascribing the strong pinning population to twin boundaries is a hypothesis, since no direct evidence of their presence is evidenced. At lower and higher temperatures there is a deviation from the fit. At low temperatures < 10 K, the dominant pinning population is the isotropic weak population, generally associated with point defects such as oxygen vacancies or atomic inclusions.

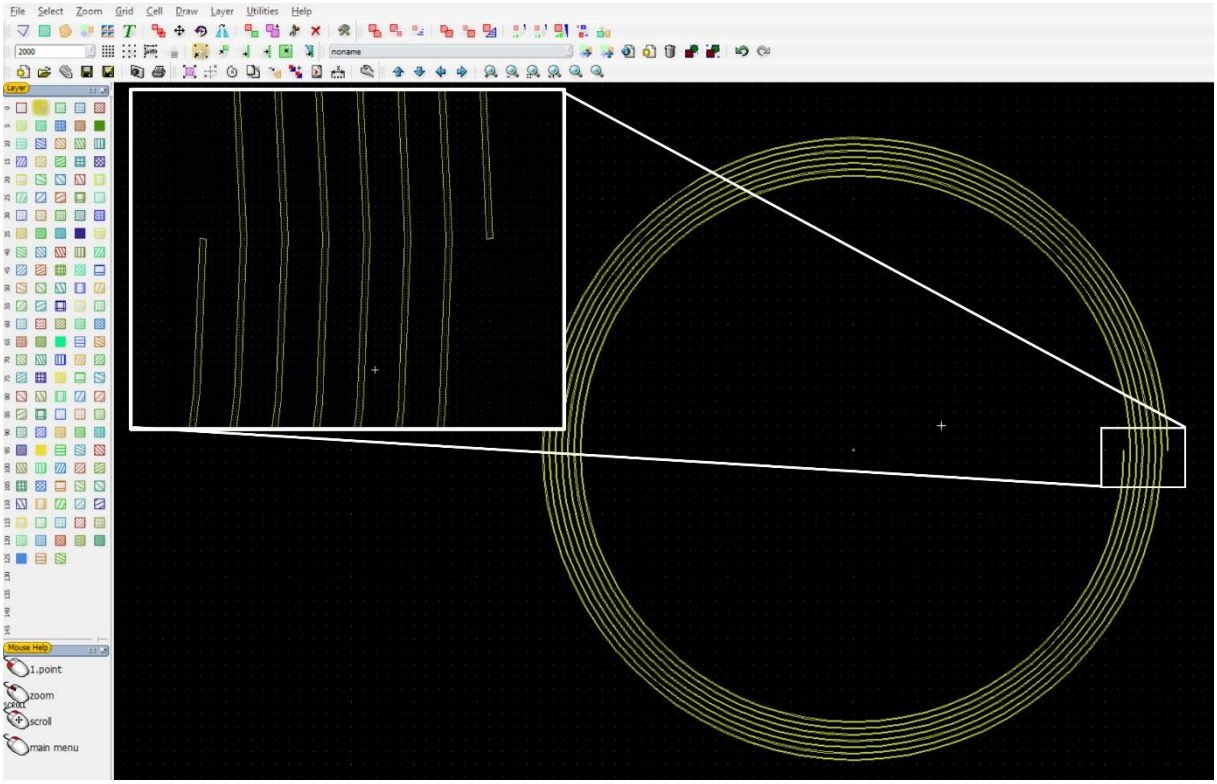

Figure 2.10 RF coil mask design and close-up.

The influence of diethanolamine used as a chelating agent in the preparation of YBCO fluorine free propionate chemical solution has been investigated. IR measurements have shown that DEA appears not to form a new complex, although complexation might differ depending on the pH value. Thermal decomposition studies for the YBCO and the YBCO-DEA precursor powders revealed their similar decomposition behavior, corresponding to a multistep mass loss with the liberation of CO_2, NO_2, H_2O and fragments corresponding to the propionate. No polymerization of the metal precursors was revealed, but the formation of bridges between $CH_3CH_2COO^-$ propionate ion groups and DEA may occur through electrostatic attraction. A more detailed analysis is needed to elucidate the nature of the DEA-precursor solution interaction. The as-obtained films, deposited on single crystal $SrTiO_3$ substrates, show a good epitaxial growth. Secondary peaks present in the ω-scan performed on the (005) YBCO peak indicate the presence of a periodicity of structural defects within the film matrix. The thermal activation energy, U, was determined. Although in self-field at 77 K, a value of ~4 MA/cm^2 was measured, the value of J_c strongly decreased when increasing the magnetic field. On the other hand, at low temperatures, the magnetic field dependence of J_c, is much better, as the power law, $J_c \propto H^{-\alpha}$, fit of the data gives a relatively low α value of 0.35. From the $J_c(T)$ curves determined at low magnetic fields, < 2T, with $H||c$, we conclude that at intermediate temperatures there is a strong pinning population, which we link to the same defect population responsible for the low intensity satellite ω-scan peaks, possibly twin boundaries. Thus, we demonstrate that the addition of DEA in propionate-

based precursor solutions for YBCO thin film deposition has a positive effect on film growth and superconducting transport performance.

RF coil UV mask design

For the fabrication of the RF coil a UV lithography mask design was developed. This mask uses a standard multi-turn receiver coil geometry. It consists of 8 turns each turn having a width of 150 µm. The outer diameter of the coil is 20 mm, while the inner diameter is 17 mm. The mask design was done using the LayoutEditor software, figure 2.10.

Estimated results and achievements

The activities of phase 2 of the project were successfully accomplished in terms of the developing of a suitable buffer layer architecture and YBCO layer deposition. The chosen methods for developing the buffer layer stack, were the inclined substrate deposition for the MgO layer and chemical solution deposition for the $LaMnO_3$ film. Our choice is motivated by the fact that these methods were successful while on the other hand are cost-effective, chemical solution deposition, and efficient, in the case of a single MgO layer deposited by inclined substrate deposition method. In terms of the YBCO layer deposition it was done by chemical solution deposition, which again was preferred as being cost-effective, time and resource-efficient. Also, as will be pointed out in the next section, the deposition of the YBCO layer was done using an original fluorine free method. The obtained results were published: *Investigation of diethanolamine (DEA) as a chelating agent in the fabrication of fluorine-free propionate route $YBa_2Cu_3O_7$ (YBCO) thin films* – A. Daniel *et al.* Supercond. Sci. Technol. **35** 054010 (2022). In terms of the RF coil fabrication we have designed a standard receiver coil for the UV lithography mask fabrication. Due to circumstances beyond our control, related to both a period of equipment break-down and repair, as well as the closing of the company that routinely provided flexible YSZ substrates (ENrG, USA) the fabrication of the RF coil on flexible substrates was not up to this point realized. Since these substrates are not routinely commercially available, their purchase is an issue. Two other manufacturers were contacted but failed to respond, Fralock (USA), Japan Fine Ceramics (Japan). However, it needs to be pointed out that the main objective of the project was to develop a set of technological thin film-related processes that would allow the fabrication of an RF coil, an objective that has been fulfilled.

3. Estimated impact and significant results

The aim of the present project was to elaborate a set of fabrication steps from a materials science point of view that would allow the elaboration of a RF coil deposited on a flexible ceramic substrate. The proposed steps, were the planarization of a flexible YSZ substrate, the deposition of a suitable buffer layer architecture ($MgO/LaMnO_3$) and the growth of an epitaxial, superconducting $YBa_2Cu_3O_7$

thin film. Regarding the planarization step we have tackled different approaches to achieve aour goal, the reduction of the substrate roughness. These approaches included the study of two alternative substrates, alumina and YSZ, modification of the Y_2O_3 precursor solution by the addition of glycerol, and substrate functionalization. The RMS roughness of the Y_2O_3 layer deposited on the functionalized YSZ substrate was of approx. 5 nm. This value is sufficiently low for a succesful deposition of the buffer layer architecture. It is to be noted that this approach, using surface functionalization, represents an original approach for planarization. In terms of the buffer layer architecture, the results encouraging, as we obtained an textured MgO layer and a LMO thin film with a roughness of 2,3 nm. This very low value ensures that the buffer layer structure is suitable, from a morphology perspective, for the superconducting layer growth. In terms of the YBCO layer deposition, we have proposed an original approach in terms of the chemical solution deposition of these type of films. We consider this to be the most important scientific result. The addition of DEA as a chelating agent in the precursor solution has proven to be effective in obtaining good quality YBCO thin films. The morphologic, structural and superconducting properties were extensively studied. The value of our study was confirmed by its publication in one of the leading journals in the field of supeconductivity, Superconductor Science and Technology: A. Daniel, M. Nasui, T. Petrisor Jr., R. B. Sonher, A. Augieri, C. Pop, A. Palau, A. Vannozzi, G. Celentano, L. Ciontea, and T. Petrisor *Investigation of diethanolamine (DEA) as a chelating agent in the fabrication of fluorine-free propionate route $YBa_2Cu_3O_7$ (YBCO) thin films* Supercond. Sci. Technol. **35** 054010 (2022) (doi: 10.1088/1361-6668/ac6298).

All relevant information pertaining to this project may be found on the project web-site: supraflex.weebly.com

Project Coordinator,

Traian Petrișor